Journal of Materials Chemistry A

Accepted Manuscript

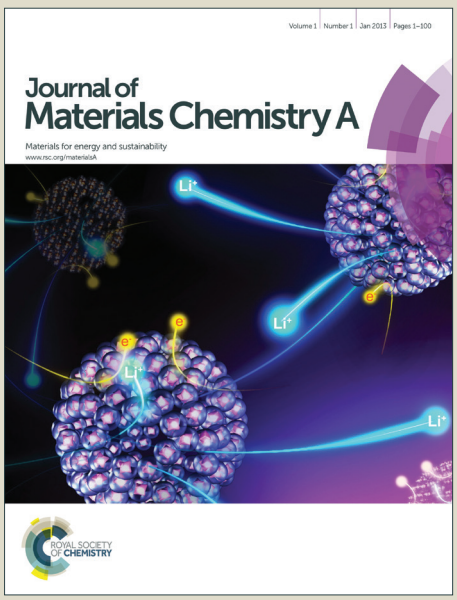

ROYAL SOCIETY OF CHEMISTRY

www.rsc.org/materialsA

Graphical Abstract

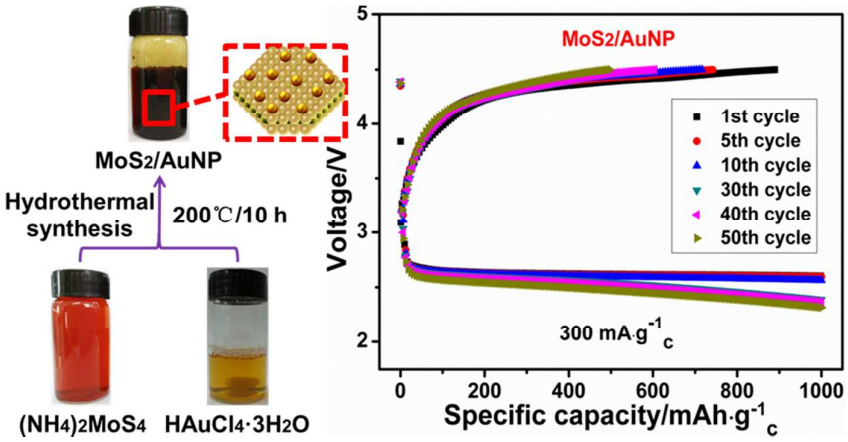

MoS_2 nanosheets decorated with gold nanoparticles show enhanced specific capacity and cycle efficiency for rechargeable Li-O_2 batteries.

Journal Name

COMMUNICATION

MoS_2 nanosheets decorated with gold nanoparticles for rechargeable Li-O_2 batteries†

Received 00th January 20xx,
Accepted 00th January 20xx

DOI: 10.1039/x0xx00000x

www.rsc.org/

Panpan Zhang,[‡a] Xueyi Lu,[‡b,c] Ying Huang,[a] Junwen Deng,[b,c] Lin Zhang,[b] Fei Ding,[*b] Zhiqiang Su,[*a] Gang Wei[*d] and Oliver G. Schmidt[b,c]

We demonstrate here a facile one-step hydrothermal synthesis to prepare molybdenum disulfide nanosheets decorated with gold nanoparticles (MoS_2/AuNP) for rechargeable Li-O_2 batteries. The fabricated Li-O_2 battery exhibits enhanced specific capacity and cycle efficiency, which are ascribed to the two-dimensional structure of MoS_2/AuNP nanohybrids and the synergistic catalytic effects of both MoS_2 nanosheets and AuNPs.

Rechargeable lithium-oxygen (Li-O_2) batteries with high theoretical specific energy density have shown enormous scientific and technological applications.[1,2] According to the overall electrochemical reaction ($2Li^+ + O_2 + 2e^- \leftrightarrow Li_2O_2$, 2.96 V vs. Li^+/Li), both oxygen reduction reaction (ORR) and oxygen evolution reaction (OER) are the two main processes during the rechargeable process.[3-5] Though much advance has been made, the application of rechargeable Li-O_2 batteries is still prevented by some challenges or problems such as poor cyclability, low energy efficiency and poor stability.[6-8] To overcome these problems, many efforts have been performed, in which the easiest and most popular solution is using a catalyst to promote the catalytic activities of electrode materials.[9-15] Many catalysts, such as non-noble metals,[9] metal compounds,[10,11] noble metals,[12-14] and carbon materials,[15] have been used for the cathode catalysts of Li-O_2 batteries in order to reduce the overpotential, facilitate the reaction process, and suppress the decomposition of the electrolyte.

Inspired by the great success of graphene materials, recently other two-dimensional (2D) graphene-like transition metal dichaleogenides (TMDs) like WS_2, TiS_2, and MoO_3 have been synthesized and utilized for various applications.[16-18] TMD nanosheets exhibit unusual properties and offer a broad view of study due to their high surface area, controlled exposed crystal facets, and diverse compositions. As a member of the TMD family, molybdenum disulfide (MoS_2) possesses excellent thermal stability and high electrocatalytic activity, which enable its wide applications such as biosensor,[19] electrocatalyst,[20,21] supercapacitor,[22,23] and energy storage.[24,25] Hybridization of MoS_2 nanosheets with noble metals, metal oxides, and carbon materials is an ideal strategy to overcome the weaknesses and optimize the performances of MoS_2 for electronic devices.[26-30] For example, Singh *et al.* produced layered free-standing papers composed of acid-exfoliated few-layer MoS_2 and reduced graphene oxide flakes for using as a self-standing flexible electrode in sodium-ion battery.[30] Recently, Bruce *et al.* improved the performances of Li-O_2 battery with dimethyl sulfoxide by using the porous Au as an cathode.[7] A synergistic catalytic effect between MoS_2 and gold nanoparticles (AuNPs) has been achieved for a highly efficient ORR.[31] The catalytic behavior of AuNPs in the ORR has already been fully investigated.[31-35] For instance, Li and co-workers developed a facile strategy to construct a AuNP film decorated with MoS_2 nanoparticles and found that the fabricated catalytic interface shows a synergistic effect on the ORR process.[31]

In this work, to know the combined advantages of AuNPs and MoS_2 nanosheets, for the first time we synthesized a novel MoS_2 nanosheets decorated with AuNPs (MoS_2/AuNP) through a facile one-step hydrothermal synthesis, and further explore the potential application of the synthesized MoS_2/AuNP as a promising cathode material for Li-O_2 battery.

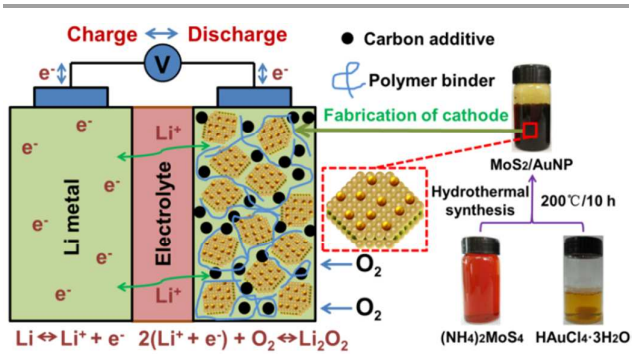

Fig. 1 Schematic presentation of the one-step hydrothermal synthesis of MoS_2 nanosheets decorated with AuNPs for rechargeable Li-O_2 batteries.

[a] State Key Laboratory of Chemical Resource Engineering, Beijing University of Chemical Technology, 100029, Beijing, China. E-mail: suzq@mail.buct.edu.cn
[b] Institute for Integrative Nanosciences, IFW-Dresden, Helmholtzstrasse 20, 01069 Dresden, Germany. E-mail: f.ding@ifw-dresden.de
[c] Material Systems for Nanoelectronics, Chemnitz University of Technology, Reichenhainerstrasse 70, 09107 Chemnitz, Germany.
[d] Faculty of Production Engineering, University of Bremen, D-28359 Bremen, Germany. E-mail: wei@uni-bremen.de
† Electronic Supplementary Information (ESI) available: Experimental details and supplementary figures. See DOI: 10.1039/x0xx00000x
‡ These authors contributed equally to this work.

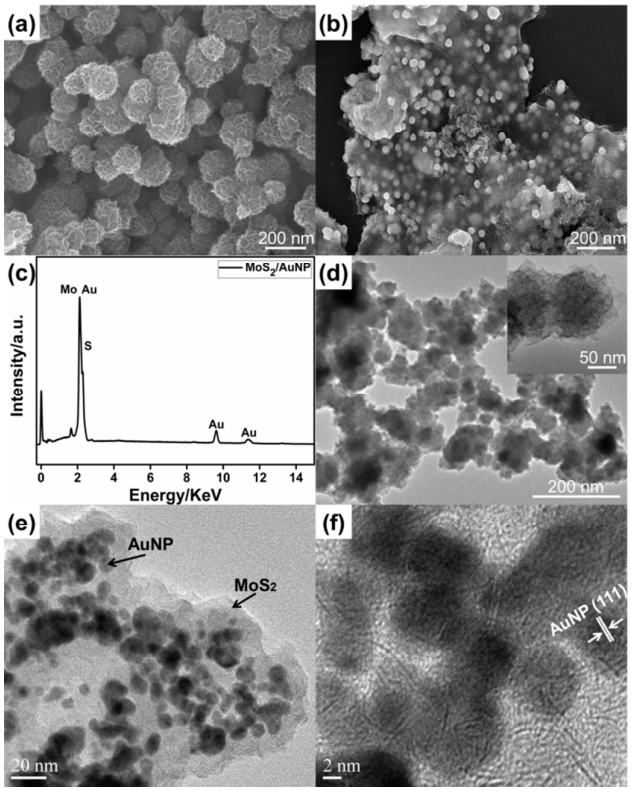

Fig. 2 Morphological and elemental characterizations: (a, d) SEM and TEM images of MoS_2 nanoflowers, (b) SEM, (c) EDX, and (e, f) HR-TEM images of MoS_2/AuNP nanohybrids.

Fig. 1 shows the synthesis strategy of MoS_2/AuNP nanohybrids and the potential reaction mechanism of a Li-O_2 battery. We utilized hydrazine to reduce $(NH_4)_2MoS_4$ and $HAuCl_4$ synchronously in an aqueous solution at 200 ^oC by a one-step hydrothermal reaction to prepare MoS_2/AuNP nanohybrids (the experimental details are provided in Electronic Supplementary Information). During this process, the $HAuCl_4$ precursor was reduced to AuNPs, which are attached onto the MoS_2 nanosheets produced by the synchronous reduction of $(NH_4)_2MoS_4$ precursor with S-Au bond. Our strategy for producing MoS_2/AuNP material has several advantages, such as economic, highly-efficient, and simple.

The morphology of the as-prepared MoS_2/AuNP nanohybrids was characterized with scanning electron microscopy (SEM) and high resolution transmission electron microscopy (HR-TEM). Fig. 2a shows the typical SEM image of pure MoS_2 synthesized in a hydrothermal system without adding $HAuCl_4$ precursors. The created MoS_2 are uniform nanoflowers with a size of 100-150 nm. The folded feature can be clearly seen, which can be confirmed by the corresponding TEM image in Fig. 2d and the corresponding inset. After adding $HAuCl_4$ precursors to the reaction system, the size of MoS_2 nanostructures decreased and the morphology of MoS_2 was transferred from nanoflowers to nanosheets, as shown in the SEM image (Fig. 2b). The corresponding TEM image indicates that the synthesized MoS_2 nanosheets were uniformly decorated with AuNPs (Fig. 2e). The morphological difference highlights the important role of AuNPs as a novel inhibitor material for mediating the growth of layered MoS_2-related nanomaterials.

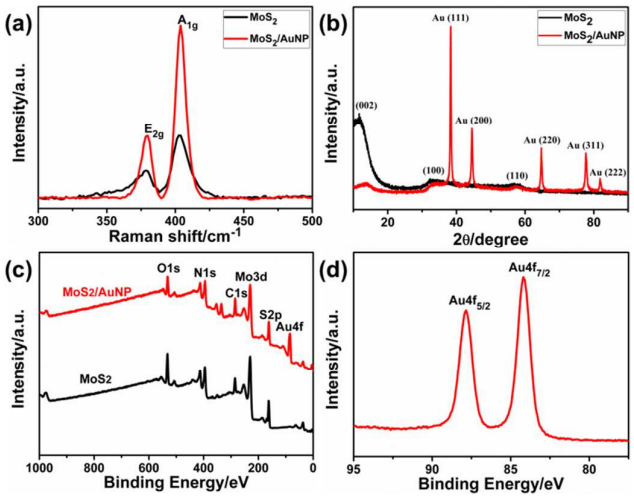

Fig. 3 Property and structure characterizations of MoS_2 nanoflowers and MoS_2/AuNP nanohybrids: (a) Raman spectra, (b) XRD patterns, and (c, d) XPS spectra.

Energy dispersive X-ray spectroscopy (EDX) was used to characterize the elemental composition of the synthesized MoS_2/AuNP nanohybrids (Fig. 2c). It is found that the signals from all three elements, Au, Mo, and S, were detected clearly. The size of AuNPs for the decoration of MoS_2 nanosheets is calculated to be about 10 nm and the HR-TEM image of MoS_2/AuNP nanohybrids demonstrates the (111) lattice face of AuNPs (Fig. 2f).

The structural characterizations of the synthesized MoS_2 nanoflowers and MoS_2/AuNP nanohybrids were then performed with Raman spectroscopy, X-ray diffraction (XRD), and X-ray photoelectron spectroscopy (XPS). As shown in Fig. 3a, Raman spectrum of MoS_2 reveals characteristic peaks of MoS_2 at 379.0 and 403.5 cm^{-1}, which agree well with the previously reported data.[36,37] In addition, the intensities of the two bands in the spectrum of MoS_2/AuNP nanohybrids are enhanced by ~250%. This low enhancement for the MoS_2/AuNP nanohybrids indicates the presence of a chemical interaction or bonding between MoS_2 and AuNPs.[38] Fig. 3b presents the XRD patterns of the prepared MoS_2 nanoflowers and MoS_2/AuNP nanohybrids. Both samples possess the broad diffraction peaks of MoS_2 nanosheets, which reveal the typical crystal domains with hexagonal structure (JCPDS card No. 47-1320). In addition, five strong diffraction peaks for MoS_2/AuNP nanohybrids are observed, which could be associated with the (111), (200), (220), (311), and (222) planes of the synthesized AuNPs.[14] Fig. 3c presents the XPS spectra of MoS_2 nanoflowers and MoS_2/AuNP nanohybrids. For both samples, the bands located at 285.0, 393.5, and 532.0 eV are associated to the characteristic peaks of C 1s, N 1s, and O 1s, respectively. In addition, the Mo 3d shows two peaks at 232.0 (Mo $3d_{3/2}$) and 228.7 eV (Mo $3d_{5/2}$), while the S 2p locates at 162.8 (S $2p_{1/2}$) and 161.7 eV (S $2p_{3/2}$), as shown in Fig. S1. The Mo and S binding energies are consistent very well with each other, indicating that the decoration of MoS_2 nanosheets with AuNPs does not change the crystallinity of MoS_2, and the MoS_2 nanosheets are chemically stable with $HAuCl_4$ solution.[27] Fig. 3d shows the Au 4f spectrum, and the peaks shown in 87.8 (Au $4f_{5/2}$) and 84.2 eV (Au $4f_{7/2}$) provide direct evidence for the formation of AuNPs on MoS_2 nanosheets.[14] On the basis of the N_2 adsorption-

desorption measurement, the specific surface area of the Super P and MoS_2/AuNP nanohybrids were calculated to be about 62.0 and 213.6 $m^2 \cdot g^{-1}$, respectively (Fig. S2a). The high surface area of MoS_2/AuNP nanohybrids can be ascribed to the binding of dense and small AuNPs. In addition, the pore-size distributions of Super P and MoS_2/AuNP nanohybrids show the similar pore size, which may benefit for lithiation and delithiation (Fig. S2b).

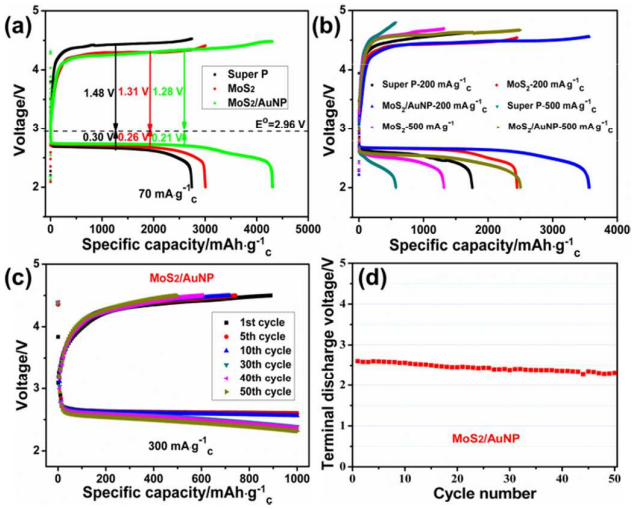

Fig. 4 Li-O_2 battery performance: (a) Discharge/charge profiles of the Li-O_2 battery with the pristine Super P, MoS_2 nanoflowers, and MoS_2/AuNP nanohybrids at a current density of 70 $mA \cdot g^{-1}_c$. (b) The first discharge/charge profiles of the Li-O_2 battery with Super P, MoS_2 nanoflowers, and MoS_2/AuNP nanohybrids at current densities of 200 and 500 $mA \cdot g^{-1}_c$. (c) Curtailing capacity at a current density of 300 $mA \cdot g^{-1}_c$. (d) Terminal discharge voltage.

Recently, MoS_2-based nanomaterials have been found to have excellent performance in energy applications.[28-34] Taking this fact into consideration, we further investigated the performance of Li-O_2 batteries fabricated with MoS_2/AuNP nanohybrids as cathodes in a non-aqueous system.

Fig. S3 shows the cyclic voltammograms (CVs) of MoS_2 nanoflowers and MoS_2/AuNP nanohybrids. Compared with the electrode without a catalyst, the MoS_2/AuNP nanohybrid-based electrode exhibits a higher ORR onset potential (~2.9 V) and a more positive current peak. Besides, the MoS_2/AuNP nanohybrid-based electrode shows a much obvious current during anodic scans (>3.0 V). These findings indicate the effective catalytic activity of MoS_2/AuNP nanohybrid in the nonaqueous phase.[39,40] The first discharge-charge curves of the Li-O_2 battery with MoS_2/AuNP nanohybrids are compared with those with Super P and MoS_2 nanoflowers at the same current density in Fig. 4a to enable an understanding of the effect of MoS_2/AuNP nanohybrid on its ORR and OER kinetics.[41] The cell composed with Super P shows discharge and charge overpotentials of 0.30 and 1.48 V, respectively, which leads to a low round-trip efficiency. The delivered specific capacity reaches a value of 2760 $mAh \cdot g^{-1}_c$. However, the cell with MoS_2 nanoflowers presents discharge and charge overpotentials of 0.26 and 1.31 V, respectively. The delivered specific capacity achieves a relative high value of 3007 $mAh \cdot g^{-1}_c$. In contrast, the cell with MoS_2/AuNP nanohybrids exhibits discharge and charge overpotentials of 0.21 and 1.28 V, respectively, which resulted in the highest round-trip efficiency and a specific capacity of about 4336 $mAh \cdot g^{-1}_c$. The discharge voltage of the cell with MoS_2/AuNP nanohybrids was about 0.09 and 0.05 V higher than that of the cell with the pristine Super P and MoS_2 nanoflowers, suggesting that MoS_2/AuNP nanohybrids have a better ORR catalytic activity than the Super P and MoS_2 nanoflowers. Moreover, the average charge voltage for MoS_2/AuNP nanohybrids was about 4.24 V, which is substantially lower than that of the battery with pristine Super P (ca. 4.44 V) by 0.2 V and MoS_2 nanoflowers (ca. 4.27 V) by 0.03 V, which indicates the superior OER catalytic activity of MoS_2/AuNP nanohybrids over Super P and MoS_2 nanoflowers.

The effects of current density on the discharge/charge voltages were further investigated based on MoS_2/AuNP nanohybrids. The AuNPs on the surface of MoS_2 nanosheets have a crucial function in the OER, and the MoS_2 nanosheets provide facile electron conduction and support for AuNPs. The performance of Li-O_2 battery with MoS_2/AuNP nanohybrids was further investigated on the basis of the total mass of the MoS_2/AuNP nanohybrid-composite cathode. As depicted in Fig. 4b, the Li-O_2 battery with MoS_2/AuNP nanohybrids delivered a specific discharge capacity of 3567 $mAh \cdot g^{-1}_c$ and a charge capacity of 3570 $mAh \cdot g^{-1}_c$ at a current density of 200 $mA \cdot g^{-1}_c$. At a higher current density of 500 $mA \cdot g^{-1}_c$, the specific discharge capacity of MoS_2/AuNP nanohybrids decreased to 2985 $mAh \cdot g^{-1}_c$, which is much higher than that of Super P and MoS_2 nanoflowers. The improved performance can be attributed to the large specific surface area and pore structure of the layered MoS_2/AuNP nanohybrid sample, which was confirmed by the N_2-adsorption-desorption data shown in Fig. S2. In addition, the combination of MoS_2 nanosheets with high electrocatalytic activity and AuNPs with good catalytic activity displays the synergistic catalytic effect and plays an important role in the catalytic performances of the fabricated Li-O_2 batteries.

The cyclability is one of the most important indices in Li-O_2 batteries, which could be promoted when utilizing a stable electrolyte and an effective catalyst. For the cyclic tests, the cells were discharged and charged at a current density of 300 $mA \cdot g^{-1}_c$, and the cells showed good performances up to 50 cycles without apparent voltage degradation (Fig. 4c and d).[42] The capacity decay may be caused by the degradation of the electrolyte which is can be attacked by the oxygen-containing intermediates. Moreover, the exhaust of the electrolyte caused by the volatilization also contributes to the capacity decay. In addition, during the discharge/charge processes, the change of morphology and structure of MoS_2/AuNP nanohybrids can have great influences on the reversible performance. Future work will be focused on exploring a stable electrolyte.

We conducted SEM, Raman spectra and XRD analysis measurements to identify the discharge products of Li-O_2 batteries with MoS_2/AuNP nanohybrids. After discharge, many small particles aggregated on the surface of the cathode, which are considered to be Li_2O_2 (Fig. S4). Furthermore, the Raman spectrum indicates that the peaks of Li_2O_2 could be clearly observed in the discharged electrode (Fig. S5a). In addition, According to the XRD pattern (Fig. S5b), new diffraction peaks were observed for the discharged electrode, which can be reasonably assigned as the (100), (101), and (110) peaks of Li_2O_2. Furthermore, the typical diffraction peaks of MoS_2, AuNPs, and Super P can be also seen. These results

indicate that Li_2O_2, as the major discharge product, is reversibly formed in a discharging process.

Conclusions

In summary, we demonstrated a facile one-step economic hydrothermal synthesis of MoS_2/AuNP nanohybrids and investigated the potential application for the cathode of rechargeable Li-O_2 batteries. Hydrazine, as the strong reductant, can reduce $(NH_4)_2MoS_4$ and $HAuCl_4$ synchronously in an aqueous solution just by a one-step hydrothermal reaction. Compared to previous reports, our strategy for producing MoS_2/AuNP nanohybrids has several advantages, such as highly-efficient, economic, and simple. With the large specific surface area and highly exposed edges of MoS_2 nanosheets, AuNPs were attached onto them with ultrafine size. Governing by the excellent electrocatalytic activities of MoS_2 and AuNPs, the MoS_2/AuNP nanohybrids as catalyst exhibited superior Li-O_2 battery performance with low discharge overpotential, high specific capacity, and good cyclability. Therefore, we expect this one-step economic hydrothermal synthesis method can be utilized to prepare other functional materials based on layered TMD materials and metal nanoparticles, and further applied in catalysis, surface-enhanced Raman scattering, energy storage, and biosensors.

Acknowledgments

The authors gratefully acknowledge the financial support from the Fundamental Research Funds for the Central Universities (project no. ZZ1307). We also would like to thank the financial support from the Deutsche Akademische Austausch Dienst (DAAD) master's short-term scholarship for academic exchange in the Leibniz Institute for Solid State and Materials Research Dresden.

Notes and references

1 A. C. Luntz and B. D. McCloskey, *Chem. Rev.*, 2014, **114**, 11721.
2 P. G. Bruce, S. A. Freunberger, L. J. Hardwick and J. M. Tarascon, *Nat. Mater.*, 2012, **11**, 19.
3 G. Girishkumar, B. McCloskey, A. C. Luntz, S. Swanson and W. Wilcke, *J. Phys. Chem. Lett.*, 2010, **1**, 2193.
4 F. Cheng and J. Chen, *Chem. Soc. Rev.*, 2012, **41**, 2172.
5 B. Y. Xia, Y. Yan, X. Wang and X. W. (David) Lou, *Mater. Horiz.*, 2014, **1**, 379.
6 F. Li, R. Ohnishi, Y. Yamada, J. Kubota, K. Domen, A. Yamada and H. Zhou, *Chem. Commun.*, 2013, **49**, 1175.
7 Z. Peng, S. A. Freunberger, Y. Chen and P. G. Bruce, *Science*, 2012, **337**, 563.
8 S. H. Oh and L. F. Nazar, *Adv. Energy Mater.*, 2012, **2**, 903.
9 J. Wu, H. W. Park, A. Yu, D. Higgins and Z. Chen, *J. Phys. Chem. C*, 2012, **116**, 9427.
10 Q. Liu, J. Xu, Z. Chang and X. Zhang, *J. Mater. Chem. A*, 2014, **2**, 6081.
11 A. Débart, A. J. Paterson, J. Bao and P. G. Bruce, *Angew. Chem. Int. Ed.*, 2008, **47**, 4521.
12 Y. C. Lu, Z. Xu, H. A. Gasteiger, S. Chen, K. Hamad-Schifferli and Y. Shao-Horn, *J. Am. Chem. Soc.*, 2010, **132**, 12170.
13 Y. C. Lu, Z. Xu, H. A. Gasteiger, S. Chen, K. Hamad-Schifferli and Y. Shao-Horn, *J. Am. Chem. Soc.*, 2010, **132**, 12170.
14 P. Zhang, Y. Huang, X. Lu, S. Zhang, J. Li, G. Wei and Z. Su, *Langmuir*, 2014, **30**, 8980.
15 Z. L. Wang, D. Xu, J. J. Xu, L. L. Zhang and X. B. Zhang, *Adv. Funct. Mater.*, 2012, **22**, 3699.
16 X. Huang, Z. Zeng and H. Zhang, *Chem. Soc. Rev.*, 2013, **42**, 1934.
17 H. Wang, H. Feng and J. Li, *Small*, 2014, **10**, 2165.
18 M. Pumera, Z. Sofer and A. Ambrosi, *J. Mater. Chem. A*, 2014, **2**, 8981.
19 T. Wang, H. Zhu, J. Zhuo, Z. Zhu, P. Papakonstantinou, G. Lubarsky, J. Lin and M. Li, *Anal. Chem.*, 2013, **85**, 10289.
20 D. Y. Chung, S. K. Park, Y. H. Chung, S. H. Yu, D. H. Lim, N. Jung, H. C. Ham, H. Y. Park, Y. Piao, S. J. Yoo and Y. E. Sung, *Nanoscale*, 2014, **6**, 2131.
21 J. Xie, H. Zhang, S. Li, R. Wang, X. Sun, M. Zhou, J. Zhou, X. W. (David) Lou and Y. Xie, *Adv. Mater.*, 2013, **25**, 5807.
22 X. Wang, J. Ding, S. Yao, X. Wu, Q. Feng, Z. Wang and B. Geng, *J. Mater. Chem. A*, 2014, **2**, 15958.
23 L. Zhang, H. B. Wu, Y. Yan, X. Wang and X. W. (David) Lou, *Energy Environ. Sci.*, 2014, **7**, 3302.
24 Z. Hu, L. Wang, K. Zhang, J. Wang, F. Cheng, Z. Tao and J. Chen, *Angew. Chem. Int. Ed.*, 2014, **53**, 1.
25 T. Stephenson, Z. Li, B. Olsen and D. Mitlin, *Energy Environ. Sci.*, 2014, **7**, 209.
26 X. Hong, J. Liu, B. Zheng, X. Huang, X. Zhang, C. Tan, J. Chen, Z. Fan and H. Zhang, *Adv. Mater.*, 2014, **26**, 6250.
27 Y. Shi, J. K. Huang, L. Jin, Y. T. Hsu, S. F. Yu, L. J. Li and H. Y. Yang, *Sci. Rep.*, 2013, **3**, 1839.
28 Y. Chen, B. Song, X. Tang, L. Lu and J. Xue, *Small*, 2014, **10**, 1536.
29 K. Chang and W. Chen, *ACS Nano*, 2011, **5**, 4720.
30 L. David, R. Bhandavat and G. Singh, *ACS Nano*, 2014, **8**, 1759.
31 T. Wang, J. Zhuo, Y. Chen, K. Du, P. Papakonstantinou, Z. Zhu, Y. Shao and M. Li, *ChemCatChem*, 2014, **6**, 1877.
32 T. Wang, D. Gao, J. Zhuo, Z. Zhu, P. Papakonstantinou, Y. Li and M. Li, *Chem. Eur. J.*, 2013, **19**, 11939.
33 X. R. Li, M. C. Xu, X. L. Li, J. J. Xu and H. Y. Chen, *J. Mater. Chem. A*, 2014, **2**, 1697.
34 F. B. Wang, J. Wang, L. Shao, Y. Zhao and X. H. Xia, *Electrochem. Commun.*, 2014, **38**, 82.
35 P. Quaino, N. B. Luque, R. Nazmutdinov, E. Santos and W. Schmickler, *Angew. Chem. Int. Ed.*, 2012, **51**, 12997.
36 Y. Li, H. Wang, L. Xie, Y. Liang, G. Hong and H. Dai, *J. Am. Chem. Soc.*, 2011, **133**, 7296.
37 B. G. Rao, H. S. S. R. Matte and C. N. R. Rao, *J. Clust. Sci.*, 2012, **23**, 929.
38 T. S. Sreeprasad, P. Nguyen, N. Kim and V. Berry, *Nano Lett.*, 2013, **13**, 4434.
39 L. Yang, S. Wang, J. Mao, J. Deng, Q. Gao, Y. Tang and O. G. Schmidt, *Adv. Mater.*, 2013, **25**, 1180.
40 L. Zhang, S. Zhang, K. Zhang, G. Xu, X. He, S. Dong, Z. Liu, C. Huang, L. Gu and G. Cui, *Chem. Commun.*, 2013, **49**, 3540.
41 Z. Jian, P. Liu, F. Li, P. He, X. Guo, M. Chen and H. Zhou, *Angew. Chem. Int. Ed.*, 2014, **53**, 442.
42 Z. Zhang, L. Su, M. Yang, M. Hu, J. Bao, J. Wei and Z. Zhou, *Chem. Commun.*, 2014, **50**, 776.